Vol. 24 • No. 30 • August 13 • 2014

www.afm-journal.de

ADVANCED FUNCTIONAL MATERIALS

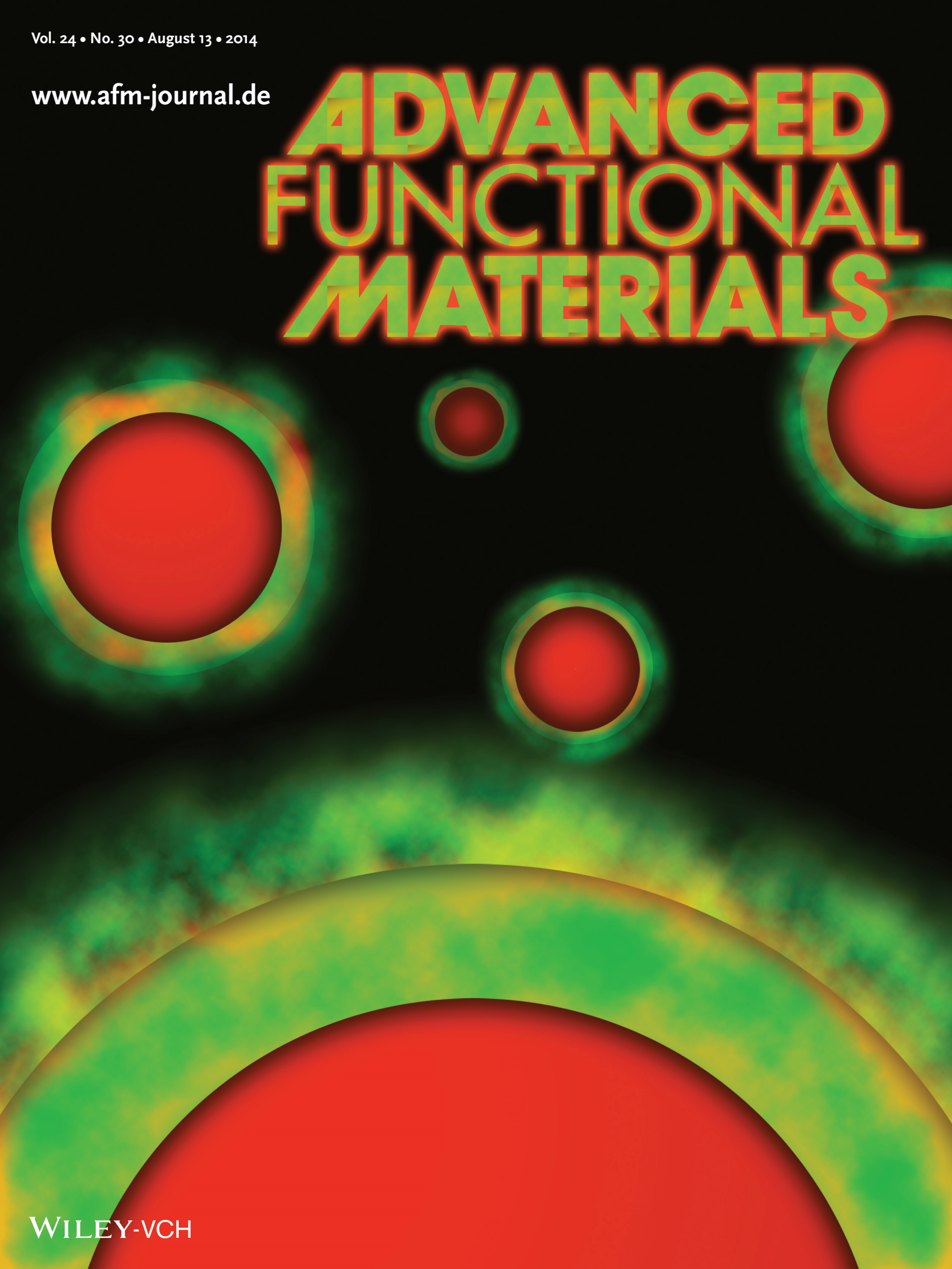

WILEY-VCH

ADVANCED FUNCTIONAL MATERIALS
www.afm-journal.de

Polymer Nanoparticles Encased in a Cyclodextrin Complex Shell for Potential Site- and Sequence-Specific Drug Release

*Guillermo U. Ruiz-Esparza, Suhong Wu, Victor Segura-Ibarra, Francisca E. Cara, Kurt W. Evans, Miljan Milosevic, Arturas Ziemys, Milos Kojic, Funda Meric-Bernstam, Mauro Ferrari, and Elvin Blanco**

Time-staggered combination chemotherapy strategies show immense potential in cell culture systems, but fail to successfully translate clinically due to different routes of administration and disparate formulation parameters that preclude a specific order of drug presentation. A novel platform consisting of drug-containing PLGA polymer nanoparticles, stably fashioned with a shell composed of drug complexed with cationic cyclodextrin, capable of releasing drugs time- and sequence-specifically within tumors is designed. Morphological examination of nanoparticles measuring 150 nm highlight stable and distinct compartmentalization of model drugs, rhodamine and bodipy, within the core and shell, respectively. Sequential release is observed in vitro, owing to cyclodextrin shell displacement and subsequent sustained release of core-loaded drug, kinetics preserved in breast cancer cells following internalization. Importantly, time-staggered release is corroborated in a murine breast cancer model following intravenous administration. Precise control of drug release order, site-specifically, potentially opens novel avenues in polychemotherapy for synergy and chemosensitization strategies.

1. Introduction

Combination chemotherapy represents a mainstay treatment modality essential for improvement of survival rates in breast cancer. However, despite numerous regimens employed clinically, patient responses following polychemotherapy remain dismal.[1] Recent molecular insights into underlying signaling pathways and networks suggest that drug synergy in combination chemotherapy may be significantly enhanced if the order of administration, scheduling, and dose duration are given proper consideration.[2,3] By delivering agents in a time- and sequence-dependent manner, it may be possible to rewire apoptotic pathways, with one drug chemosensitizing cancer cells to a second drug.[4] Strategies where agents are delivered sequentially may also serve to inhibit feedback loops and survival mechanisms inherent to complex signaling cascades by targeting multiple components along the same pathway.[5]

While specific combinations of drugs delivered in a time-staggered fashion have been shown to synergistically enhance cell killing preclinically in cell culture systems, this strategy does not translate successfully to the clinic. Pharmacokinetic limitations of conventional drug formulations, including short circulation half-lives and heightened volumes of distribution,[6] result in non-specific accumulation of drugs in healthy tissues and insufficient bioavailability in tumors. Moreover, different routes of administration, as well as distinct excipients associated with individual formulations of conventional drugs, result in disparate pharmacokinetic parameters that preclude adherence to strict time constraints specifically in tumors,[7] thereby negating therapeutic crosstalk between synergistic agents.

Nanoparticle preparations of traditional chemotherapeutics have substantially improved the pharmacokinetic limitations of agents such as doxorubicin[8] and paclitaxel.[9] Encapsulating drugs in nanoscale carriers aids in evasion of sequestration by the reticuloendothelial system (RES), with ensuing increased circulation times resulting in improved nanoparticle accumulation in tumors through the enhanced permeability and retention (EPR) effect.[10,11] Past research efforts have

G. U. Ruiz-Esparza, S. Wu, V. Segura-Ibarra, F. E. Cara, A. Ziemys, M. Kojic, M. Ferrari, E. Blanco
Department of Nanomedicine
The Houston Methodist Research Institute
Houston, TX 77030, USA
E-mail: eblanco@HoustonMethodist.org
G. U. Ruiz-Esparza, V. Segura-Ibarra
Escuela de Biotecnología y Alimentos
Escuela de Medicina y Ciencias de la Salud
Instituto Tecnológico y de Estudios Superiores de Monterrey
Monterrey, NL 64849, MX

DOI: 10.1002/adfm.201400011

K. W. Evans, F. Meric-Bernstam
Department of Investigational Cancer Therapeutics
The University of Texas MD Anderson Cancer Center
Houston, TX 77030, USA
M. Milosevic, M. Kojic
Bioengineering Research and Development Center
Belgrade Metropolitan University
Kragujevac 34000, SRB
M. Ferrari
Department of Biomedical Engineering
Weill Cornell Medical College
New York, NY 10021, USA

ADVANCED FUNCTIONAL MATERIALS
www.afm-journal.de

focused on the co-encapsulation of drugs within nanoparticles in attempts to enhance synergistic cell killing.[12] However, the focus has remained largely on amassing two or more drugs in the tumor with minimal regard for inter-drug synergistic effects, save for a few notable examples.[13] Once at the tumor site, release from nanoparticles is dictated by diffusivity parameters and hydrophobicities of drugs, with little to no control over order of drug presentation. As a result, innovative nanoparticles and delivery vectors have emerged with time-staggered drug release kinetics,[14] highlighting the importance of incorporating time and sequential delivery design parameters into the nanoplatform to ensure maximum synergistic efficacy.

Herein, we designed a novel nanoparticle platform capable of releasing synergistic agents in a time- and sequence-dependent manner, site-specifically in tumors (**Figure 1**). The nanoconstruct, called nested nanoparticles (NNP), consists of a drug-containing polymeric core, composed of poly(lactic-co-glycolic acid) (PLGA), surrounded by an outer shell composed of drug complexed with cationic cyclodextrin (QAβ-CD). PLGA was chosen as the material of the core-forming nanoparticle due to its ability to encapsulate hydrophobic agents.[15] Cyclodextrins (CDs) are cyclic oligosaccharides in the form of truncated cones, and were chosen as the shell forming material because of their ability to form inclusion complexes with hydrophobic drugs, effectively increasing their water solubility.[16] The nanoplatform comprises a system with independent dual-release kinetics due to the combination of two stand-alone delivery vectors within a single nanoconstruct. Thus, the system represents a departure from current nanoformulations that simply co-encapsulate multiple drugs within a core and are dependent on innate diffusivity parameters for drug presentation. Sequential release of drug from the outer shell followed by release of drug from the nanoparticle core, site-specifically in tumors, stands to significantly impact synergy enhancement in chemotherapy, providing an avenue for successful translation of preclinical time-staggered strategies.

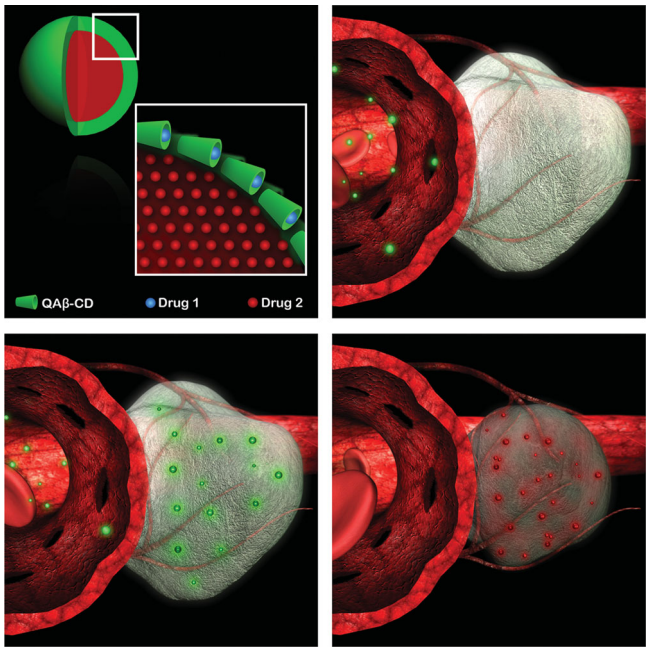

Figure 1. Nested nanoparticles designed for time and sequential release of synergistic therapeutics site-specifically in tumors. The proposed platform consists of drug-containing PLGA nanoparticles with an outer shell composed of drug complexed with cyclodextrin (QAβ-CD). Following intravenous administration, nanoparticles are hypothesized to accumulate in tumors through the enhanced permeability and retention (EPR) effect. Once at the site, drug in the outer shell is released during the early timepoints, chemosensitizing cancer cells to a second drug released at later timepoints from the nanoparticle core, resulting in synergistic enhancement of tumor cell killing.

2. Results and Discussion

2.1. Examination of Adhesion Force Between QAβ-CD and PLGA

A firm and stable adhesion between the shell-forming material, QAβ-CD, and PLGA nanoparticles proved critical towards the overall success of the proposed platform. It was initially hypothesized that electrostatic interactions between the positively charged quaternary ammonium associated with QAβ-CD and the negatively charged PLGA surface would provide a stable core-shell construct. Therefore, nanoindentation experiments using atomic force microscopy (AFM) were performed to measure the adhesive force between the component parts, employing tips modified with QAβ-CD and a surface covered with PLGA nanoparticles (**Figure 2**a). As can be observed in the AFM image comprising Figure 2b, the substrate was comprehensively overlaid with PLGA nanoparticles. Figure 2c comprises force-distance curves achieved from pull-off experiments between the QAβ-CD-coated AFM tip and PLGA nanoparticles and control substrates. Following indentation of the PLGA and control surfaces to a desired force value, retraction of the cantilever was examined. The strong adhesion between the tip and the PLGA nanoparticles caused the cantilever to adhere to nanoparticles beyond a certain distance (i), a distance where the tip was successfully separated from control substrates. It was not until after a certain point (ii) that adhesion was broken and the AFM tip was successfully separated from the nanoparticle surface. The average adhesion force between QAβ-CD and PLGA nanoparticles, as determined by force curves in Figure 2c, was found to be approximately 8.5 ± 0.8 nN (Figure 2d). In contrast, the adhesion force measured using the same QAβ-CD-functionalized tip and a control surface containing no PLGA nanoparticles was found to be 0.4 ± 0.2 nN.

Force at the single molecule level was estimated using a technique called blind tip evaluation.[17] The tip diameter was approximated as 8 nm after immersion in QAβ-CD solution, leading to the estimation that on the apex of the tip, 6-8 QAβ-CD molecules were present on the surface. Thus, the maximum force between a single QAβ-CD molecule and PLGA was determined to be 1.1 nN. In contrast, the maximum force between a single QAβ-CD molecule and the control surface was 59.2 pN. The adhesive force between QAβ-CD and PLGA proved extremely strong, especially when compared to biological interactions in nature. As an example, Hinterdorfer and coworkers reported that the single molecule force between IgG and single strand DNA was approximately 50 pN.[18] The strong

Adv. Funct. Mater. **2014**,
DOI: 10.1002/adfm.201400011

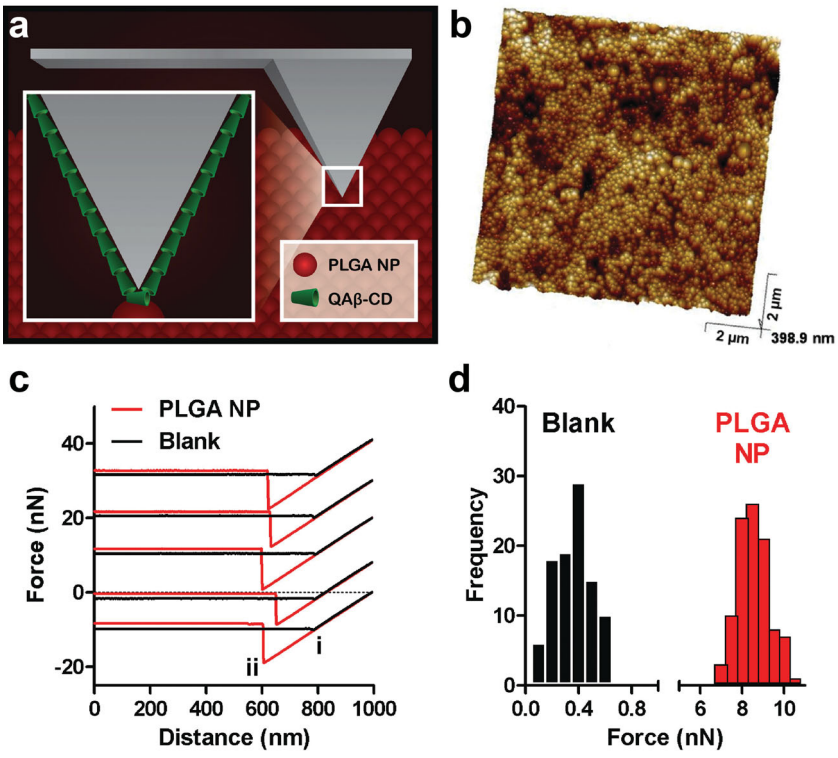

Figure 2. AFM examination of adhesive force between QA*β*-CD and PLGA. a) Schematic illustrating the QA*β*-CD-functionalized AFM tip and PLGA nanoparticles settled on the substrate. b) AFM topographical image of PLGA nanoparticles. c) Representative attractive F–D curves of positive QA*β*-CD interacting with the negative PLGA surface. Red and black traces indicate retraction (detachment) signals of the AFM tip from a PLGA nanoparticle substrate and blank substrate, respectively. The five different force curves were produced from the same QA*β*-CD-functionalized tip and are displaced vertically for clarity of presentation. d) Histogram ($n = 110$) of pull-off force values for the interaction of QA*β*-CD with PLGA nanoparticles and blank substrates obtained with the same tip.

force between QA*β*-CD and the PLGA surface is most likely a combination of ionic, Van der Waals, and molecular interaction forces. The firm adhesion between the core forming material and shell should contribute to pronounced stability of the nanoparticle upon intravenous infusion into the blood stream, preventing undesirable premature release of drugs prior to arrival at the tumor site.

2.2. Nested Nanoparticle Size and Morphology Characterization

Having verified the strong adhesion between core- and shell-forming components, the nested nanoparticle platform, comprising a drug-containing nanoparticle core coated with a shell composed of cyclodextrin-complexed drug, was fabricated and characterized. Throughout the entirety of the study, the fluorophores rhodamine and bodipy were used as model drugs for encapsulation within PLGA nanoparticles and complexation with QA*β*-CD, respectively. For ease of platform morphological and architectural analysis, specifically core-shell compartmentalization of distinct drugs, rhodamine-containing PLGA microspheres averaging 2 μm in diameter were fabricated and subsequently coated with bodipy-cyclodextrin complexes (bodipy·QA*β*-CD). Upon examination of nanoparticles via confocal microscopy, rhodamine (red) encapsulated within the PLGA core and a bodipy·QA*β*-CD shell (green) enveloping the nanoparticle were clearly discernible (**Figure 3**a). As hypothesized, the outer drug layer formed a dense uniform coating around the nanoparticle, with distinct compartmentalization of the two drugs within the system.

The morphology and architecture achieved on the microscale was expected to effectively translate towards the nanoscale, a size range beneficial for both long-term circulation[19] and accumulation in tumors through the EPR effect.[20] SEM (Figure 3b) and AFM examination demonstrated the small size and spherical morphology of nested nanoparticles, confirming their monodispersity (Figure S1, Supporting Information). Rhodamine-containing PLGA nanoparticles possessed an average diameter of 105 nm as determined by dynamic light scattering (DLS) analysis (Figure 3c). Upon addition of the bodipy·QA*β*-CD outer shell, the size of the nanoparticles increased to an average diameter of 142 nm. Analysis of the surface charge of the nanoparticles, prior to and following addition of the bodipy·QA*β*-CD shell, confirmed the presence of the cyclodextrin outer layer. As is evident in Figure 3d, the negative surface charge associated with PLGA nanoparticles (–28 mV) became highly positive (+25 mV) following the addition of bodipy·QA*β*-CD. Successful assembly of the core-shell construct was further verified via TEM, which served to corroborate the small and uniform size of the nanoparticles (Figure 3e). Magnification of nested nanoparticles under TEM demonstrated the presence of an outer layer surrounding the electron dense mass of the PLGA nanoparticle (Figure 3f). Upon subsequent analysis, the thickness of the shell was found to agree with measurements obtained by dynamic light scattering (Figure S2, Supporting Information). Upon phase-separation analysis, the ratio of PLGA:QA*β*-CD was found to be approximately 15:1.

2.3. Release Examination from Nested Nanoparticles

Figure 4 summarizes the release kinetics of rhodamine and bodipy from nested nanoparticles. As is evident in Figure 4a, minimal drug release occurred from nanoparticles in the initial timepoints leading up to 3 h (7% and 3% of bodipy and rhodamine, respectively). Nominal release at early timepoints following intravenous administration should limit accumulation of drugs in healthy tissues and organs, in turn hindering potential side effects,[21] and allow sufficient time for the nanoparticle to successfully accumulate at the site of action prior to release. After 3 h, an increase in bodipy release occurred,

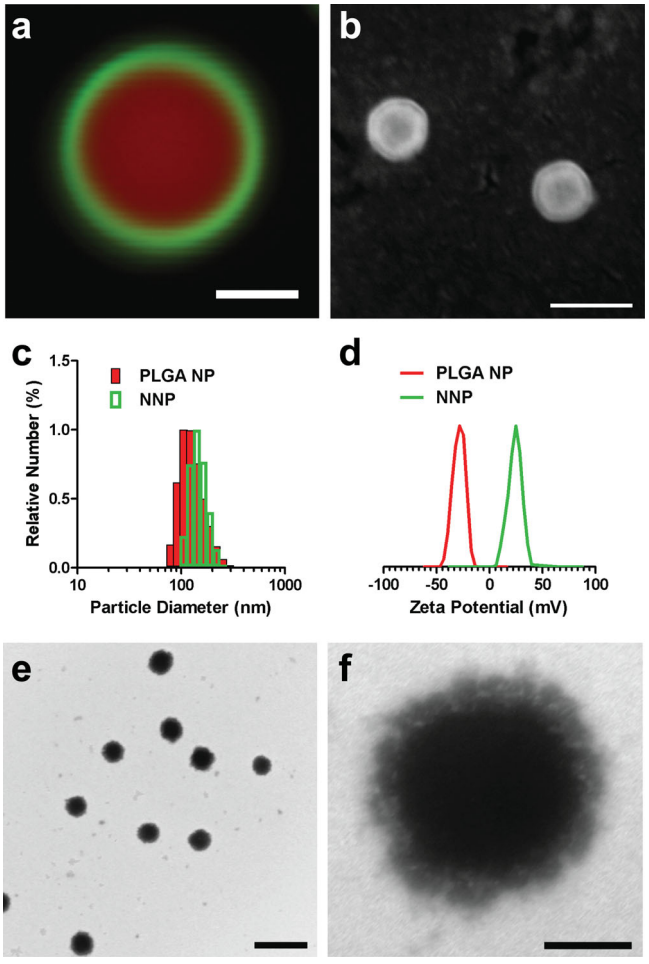

Figure 3. Nested nanoparticle characterization. a) Confocal microscopy image of a single nested particle demonstrating the core-shell compartmentalization of bodipy (green) and rhodamine (red). The scale bar represents 5 μm. b) SEM micrograph of nested nanoparticles. The scale bar represents 200 nm. c) Dynamic light scattering histogram depicting the size of nanoparticles prior to and after functionalization with the QAβ-CD shell. d) Zeta potential analysis of nanoparticles prior to and after addition of the QAβ-CD shell. e) Transmission electron microscopy image of nested nanoparticles. The scale bar represents 500 nm. f) Magnification of nested nanoparticle from e. The scale bar represents 100 nm.

reaching 34% of drug by 6 h. By 12 h, 50% of bodipy was released from nanoparticles, with release plateauing after 48 h. It is important to note that minimal release of rhodamine (≈10%) occurred by this same timepoint. Indeed, throughout the entirety of the study, rhodamine release was extremely slow and sustained, reaching merely 34% release in 96 h.

Due to the fact that the physico-chemical properties of the core and shell, as well as bodipy and rhodamine, are different, a computational method accounting for diffusivities and molecule partitioning was used to analyze release kinetics from nested nanoparticles (see Supporting Information). Use of the model helped determine that sequential release may be achieved and controlled not only by different diffusion properties in different phases, but also partitioning. Modeling results suggest that release from the core and shell saturated at 46% and 92%, respectively. The model estimated experimental

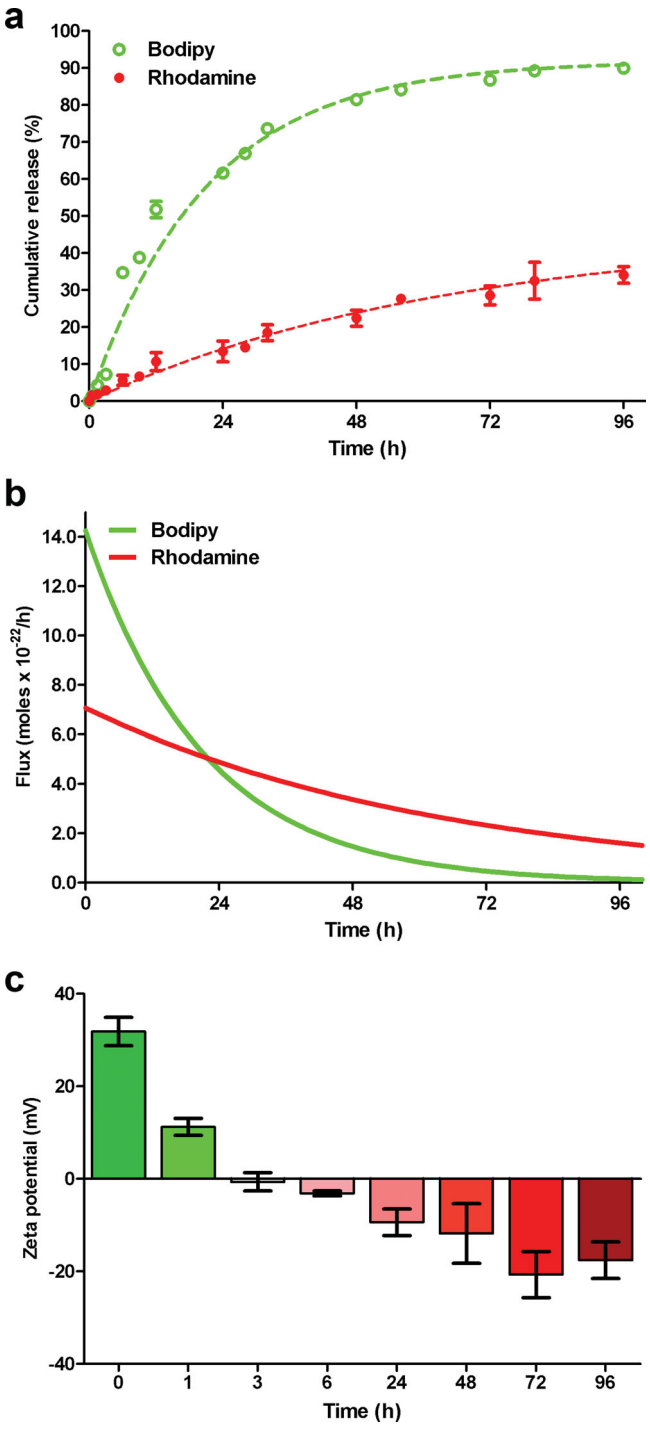

Figure 4. Examination of nested nanoparticle release kinetics. a) Cumulative release of bodipy and rhodamine from nested nanoparticles in PBS at pH 7.4 and 37 °C. Model fits to experimental data are represented by dotted lines. b) Fluxes of bodipy and rhodamine release from nested nanoparticles. c) Zeta potential examination of nested nanoparticles at specific timepoints in simulated release conditions (PBS at pH 7.4 and 37 °C).

release curves by using partitioning coefficients of 5.0×10^9 and 2.2×10^{11} for bodipy and rhodamine, respectively (Figure 4a). The half-time of release of the maximum releasable material was estimated to be 15 h for the shell and 46 h for the core. The

Adv. Funct. Mater. **2014**,
DOI: 10.1002/adfm.201400011

diffusivity of rhodamine inside the PLGA nanoparticle matrix was estimated to be 4×10^{-10} cm^2 s^{-1}, which was approximately 10^4 times lower than that in water,[22] while that of bodipy in the shell was reduced by only 5 times compared to that in water. Based on the model fit, the partitioning of both rhodamine and bodipy proved to be the most important factor influencing release kinetics, proving critical in the design of future embodiments of nested nanoparticles for sequential release. This is illustrated in the distinct phases of dominant fluxes over time (Figure 4b). The rate of release of rhodamine from nested nanoparticles was initially outperformed by bodipy release, but eventually the rhodamine flux overtook the flux of bodipy after 24 h.

Nanoparticle surface charge examination at distinct timepoints provided valuable insights into the mechanism of drug release. As apparent in Figure 4c, the nested nanoparticle platform was positively charged at the initial timepoints. However, as time progressed, the nanoparticle became less positive, with the surface charge undergoing an inflection and shift towards negative values after the 3 h timepoint. Noticeably, this coincided with the timeframe of increased release of bodipy observed in Figure 4a. At subsequent timepoints, the nanoparticle became increasingly negative, plateauing at roughly the same time as bodipy release. Taken together, the mechanism of release of bodipy from nested nanoparticles was driven primarily through detachment and displacement of cyclodextrin-complexed drug from nanoparticle surfaces. Slow release of rhodamine was primarily due to the high inherent viscosity of the PLGA polymer utilized in the study, shown previously to result in sustained release of therapeutics over time,[23] as well as partitioning that demonstrated preference of rhodamine molecules for the PLGA phase. Confocal microscopy of nested nanoparticles at distinct timepoints also highlighted the mechanism of release (Figure S3, Supporting Information). At early timepoints, nanoparticles were coated by the bodipy·QAβ-CD shell, which dissipated over time, giving way to nanoparticles with a sustained presence of rhodamine within their cores.

2.4. Examination of Nested Nanoparticle Internalization and Intracellular Sequential Release within Breast Cancer Cells

Potential cytotoxic effects stemming from the nested nanoparticle platform were examined in human primary endothelial cells via MTT assay. Nested nanoparticles did not have a detrimental effect on cell viability (Figure S4, Supporting Information), agreeing well with previously published reports on cytotoxic effects of PLGA-based systems.[24] Nanoparticle internalization and subsequent intracellular localization and drug release were examined in MCF-7 breast cancer cells (**Figure 5**). As can be observed in confocal micrographs comprising Figure 5a, nested nanoparticles underwent internalization in MCF-7 breast cancer cells after 1 h of incubation. Internalization of nested nanoparticles was likely facilitated by their positive surface charge, which has been previously shown to enhance traversal through negatively-charged membranes via endocytotic pathways.[25] Intracellular release of drugs over time was evident, with fluorescence of bodipy waning as time progressed past the 3 h timepoint. At later timepoints of 24 and 96 h, the fluourescence emanating from MCF-7 cells was primarily due to rhodamine in nanoparticles, with the majority of bodipy having been released.

Single-cell analysis (Figure 5b) provided further insights into nested nanoparticle internalization and release, as well as intracellular trafficking. By 1 h, nanoparticles have undergone association with the cell membrane, and were shown to undergo engulfment in early endosomes. At later timepoints, larger amounts of nanoparticles were internalized, leading to the formation of larger, late-stage endosomal compartments. As can be seen at timepoints of 24 and 96 h, migration of nanoparticles to the perinuclear region of the cell has occurred, with nanoparticles likely found within lysosomal bodies. Analagous to Figure 5a, bodipy and rhodamine were found to be co-localized and associated with nanoparticles at early timepoints, while at later timepoints, only rhodamine fluorescence remained, successfully demonstrating intracellular sequential drug release dynamics using the nested nanoparticle platform.

Intracellular release behavior was quantified utilizing flow cytometry analysis. As shown in Figure 5c,d, the intracellular fluorescence intensity of bodipy decreased significantly after 24 h, confirming the sequential release behavior of the nanoparticles. Contrastingly, and in agreement with in vitro and cellular studies, the release of rhodamine did not vary significantly over time, demonstrating slow and sustained release dynamics.

2.5. In Vivo Examination of Sequential Release from Nested Nanoparticles

Nested nanoparticles were designed to successfully navigate the bloodstream following intravenous administration and site-specifically accumulate in tumors, releasing its contents in a time- and sequence-dependent fashion (Figure 1). MCF-7 breast tumor xenografts from mice were examined for the presence of bodipy and rhodamine using confocal microscopy at different timepoints following intravenous administration. As can be seen in **Figure 6**a, tumor tissues show colocalization of both dyes 3 h after administration of nested nanoparticles. Surface intensity plots (Figure 6a and Supporting Information Figure S5) clearly highlight bodipy and rhodamine fluorescence, indicating accumulation of nanoparticles within the tumor at this relatively short timepoint. Importantly, these findings reinforce the stability of the nanoparticle construct following intravenous administration. Area fraction analysis of distinct regions of the tumor demonstrated that bodipy and rhodamine were found in ratiometrically similar amounts within the tumor at 3 h. In contrast, at 24 h, there was a marked decrease of bodipy in the tumor tissue (Figure 6b), as reflected in the accompanying surface intensity plot and area fraction analysis. At 96 h, confocal micrographs show that the vast majority of the tumor tissue examined emanated rhodamine-associated fluorescence, with minimal bodipy fluorescence in the tumor (Figure 6c). Area fraction analysis demonstrated an increase in rhodamine amount at this time in the tumor, while the amount of bodipy in the tumor has decreased significantly. Taken together, these results demonstrate that the nested nanoparticle platform is capable of sequential release intratumorally. Importantly, the slow intratumoral release of drug from the

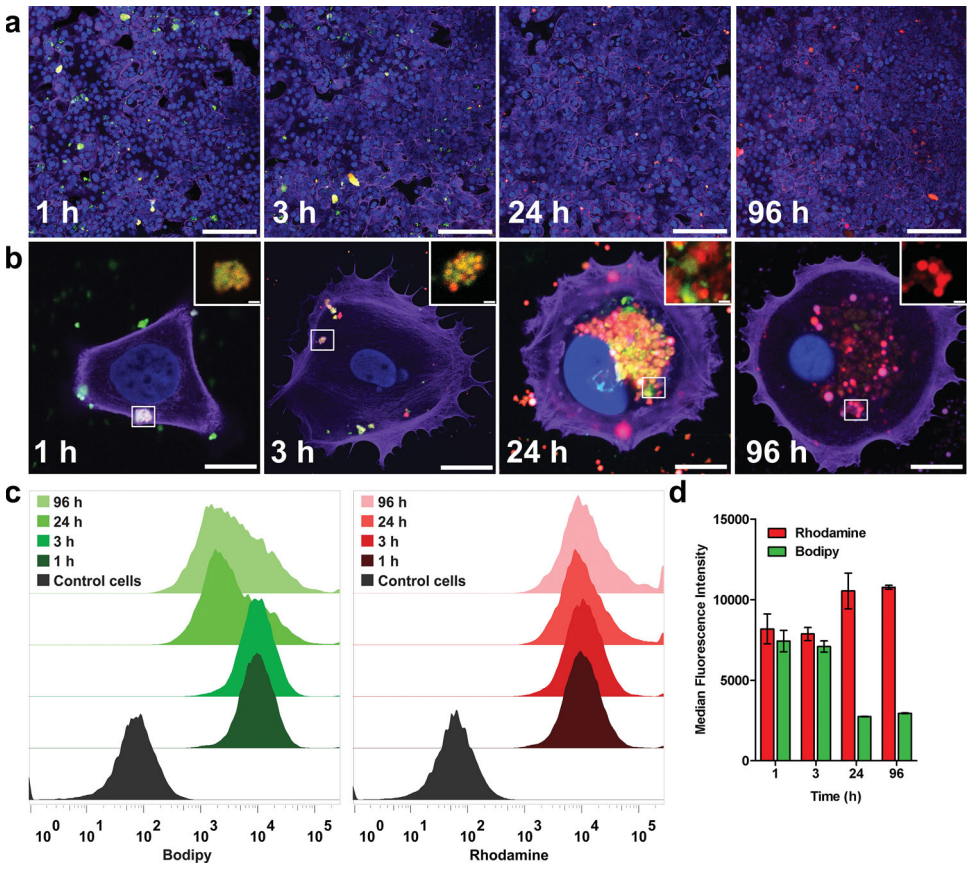

Figure 5. Internalization of nested nanoparticles and intracellular release in MCF-7 breast cancer cells. a) Confocal microscopy of MCF-7 breast cancer cells at predetermined timepoints after administration of nested nanoparticles. The green fluorescence emanates from bodipy while the red fluorescence from rhodamine. The scale bar represents 200 μm. b) Single-cell confocal microscopy examination of nested nanoparticle internalization and release at different timepoints. Green fluorescence is due to bodipy while red fluorescence denotes the presence of rhodamine. The scale bar represents 20 μm. Figure insets represent magnifications of areas outlined in boxes. The scale bars in the insets represent 1 μm. c) Flow cytometry histograms of nanoparticle accumulation over time in MCF-7 breast cancer cells. d) Mean fluorescence intensity over time in MCF-7 breast cancer cells as determined by flow cytometry analysis.

nanoparticle core observed in these studies may prove beneficial, as improved tumor efficacies have been observed following prolonged exposure to therapeutics.[10]

3. Conclusions

Site-specific delivery of multiple drugs is of paramount importance in cancer, where combination chemotherapy regimens aim to exploit synergistic cell-killing efficiency while minimizing drug resistance and adverse patient side effects. Nanoparticle-based drug delivery has successfully overcome pharmacokinetic limitations of conventional drug formulations, aptly navigating intricate biological barriers to co-deliver therapeutics to tumors. However, novel insights into molecular mechanisms governing tumorigenesis extend the notion of synergistic enhancement to order and timing of drug presentation.[2] In this study, we have developed a nanoparticle platform capable of site-specifically delivering drugs to tumors in a time- and sequence-dependent manner. We have demonstrated the formation of a highly stable nanoconstruct with sequential release behavior in vitro, a behavior that was effectively translated and preserved in cellular and in vivo models of breast cancer.

To the best of our knowledge, this is the first demonstration of intracellular and intratumoral sequential release of agents from a nanoparticle platform designed specifically for staggered release, highlighting the feasibility of the nanoparticle as a novel strategy for synergistic enhancement in cells necessitating chemosensitization, or as an approach to overcome feedback loop activation by pro-survival molecules. Hence, work is currently underway to identify potential synergistic avenues in cancer that might benefit from time- and sequence-dependent delivery of therapeutics, as well as potential drug candidates for incorporation within the nanoparticle platform. Ongoing experiments are also dedicated to modulation of release kinetics depending on optimized timing for drug synergy, as well as the possibility of tailoring the platform for multi-drug and/or genetic material (e.g., siRNA) incorporation and release. In vivo biodistribution and efficacy analyses will be performed with future incarnations of the platform that contain therapeutic agents that synergistically enhance cell-killing in a sequential fashion. Last but not least, future work will focus on extending the notion of time-staggered delivery

Adv. Funct. Mater. **2014**,
DOI: 10.1002/adfm.201400011

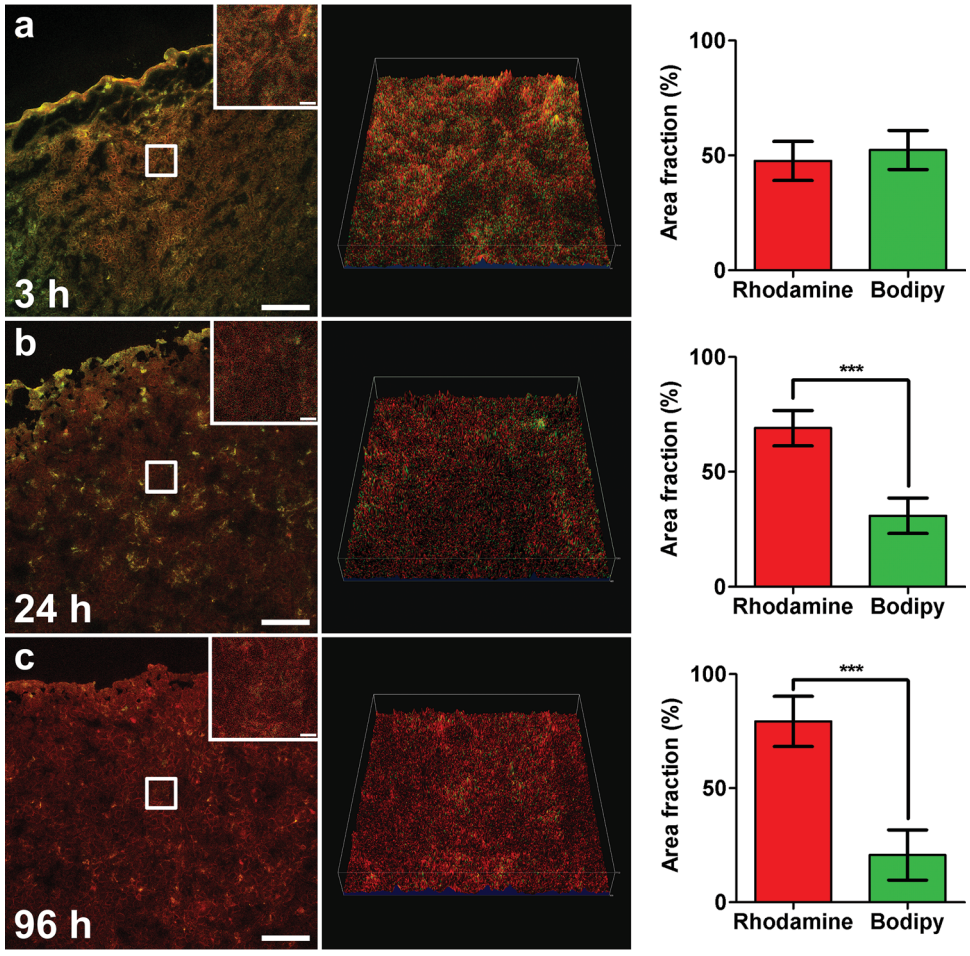

Figure 6. Nested nanoparticle accumulation in an MCF-7 murine model of breast cancer. a–c) comprise representative confocal microscopy images of excised MCF-7 tumors at 3, 24, and 96 h, respectively. Green fluorescence is due to bodipy while red fluorescence denotes the presence of rhodamine. The scale bars in the images represent 200 μm. Figure insets represent magnifications of areas outlined in boxes. The scale bars in the insets represent 20 μm. Immediately to the right of each confocal microscopy image is a fluorescence intensity plot of boxed areas in the preceding figure. The last column of the figure represents area of bodipy and rhodamine as a fraction of the total area, obtained from multiple sections (n = 4) of tumors (n = 3) at their corresponding timepoints. Asterisks (***) indicate a significance level of $p < 0.001$.

of therapeutics using nested nanoparticles to other disease conditions.

4. Experimental Section

Materials: Poly(DL-lactide-co-glycolide) 50:50 (PLGA, inherent viscosity 0.95–1.20) was purchased from Durect Corporation (Birmingham, AL). Quaternary ammonium β-cyclodextrin (QAβ-CD) was purchased from Cyclodextrin Technologies Development, Inc. (Alachua, FL). Rhodamine (λ_{ex} 554 nm; λ_{em} 627 nm) was purchased from Sigma Aldrich (St. Louis, MO). The fluorescent probe 6-(((4,4-Difluoro-5-(2-Thienyl)-4-Bora-3a,4a-Diaza-s-Indacene-3-yl) styryloxy) acetyl) aminohexanoic Acid, Succinimidyl Ester) (Bodipy; λ_{ex} of 630 nm, λ_{em} of 650 nm) was purchased from Life Technologies (Grand Island, NY). MCF-7 human breast cancer cells were obtained from the American Tissue Culture Collection (Manassas, VA). Human primary endothelial cells were obtained from Promega (Madison, WI). Cell lines were cultured in Dulbecco's modified Eagle's medium (DMEM)/F-12 (Mediatech, Inc., Manassas, VA) supplemented with 10% (v/v) FBS (Sigma Aldrich, St. Louis, MO) and maintained at 37 °C in a humidified atmosphere containing 5% CO_2 throughout the course of experimentation.

Examination of Adhesive Interaction Between PLGA Nanoparticles and Cyclodextrin: Adhesion force between QAβ-CD and PLGA was examined via AFM using a MultiMode 8 AFM (Bruker, Madison, WI, USA). Chemical modifications of QAβ-CD functionalized AFM tips and PLGA nanoparticle fixed substrates for force measurements are described in Supporting Information. Force spectroscopy measurements were conducted in liquid conditions with DI water as a buffer. Sensitivity and spring constants for the cantilever were calibrated automatically from a stable force curve. The functionalized AFM tip was manually placed over a PLGA nanoparticle film substrate to ensure an interaction between the QAβ-CD-functionalized tip and PLGA, as visualized via AFM microscopy. When the tip was in contact with the PLGA nanoparticle surface, the tip ramp model was activated, and force curves were automatically recorded on a specific spot of the PLGA surface. To confirm the reproducibility of the force curves, at least 5 spots on the PLGA nanoparticles were selected randomly.

Fabrication and Characterization of Core-Forming PLGA Nanoparticles: PLGA nanoparticles were fabricated using a modified double emulsion procedure.[26] Resulting nanoparticles were characterized for size and surface charge using a Malvern Zetasizer Nano ZS dynamic light scattering (DLS) instrument (Malvern Instruments Ltd, Worcestershire, UK). Size and morphology were verified using SEM (Nova NanoSEM 230, FEI, Hillsboro, OR, USA) and AFM. Encapsulation of rhodamine

within nanoparticles was examined using a Synergy H4 Hybrid Reader at a $\lambda_{max} = 554$ nm.

Bodipy Complexation with QAβ-CD: Bodipy was dissolved in THF, and added to a QAβ-CD aqueous solution. After stirring for 4 h, THF was allowed to evaporate overnight. The resulting suspension was centrifuged at 10,000 rpm for 5 min and filtered using a 0.45 μm filter. The concentration of bodipy following complexation with cyclodextrin was determined as described above at a $\lambda_{max} = 630$ nm.

Fabrication and Characterization of Nested Nanoparticles: Rhodamine-containing PLGA nanoparticles were incubated with bodipy·QAβ-CD complexes in solution. Following 3 h, nanoparticles were washed to remove excess bodipy·QAβ-CD. Nanoparticles were then characterized for size via DLS, SEM, and AFM, as well as surface charge, as described previously. Nanoparticle size was also characterized by transmission electron microscopy (TEM) using a JEM-1210 TEM (JEOL, USA, Inc., Peabody, MA). The ratio of PLGA to cyclodextrin in the platform was determined following dissolution of nested nanoparticles in dichloromethane and water, so as to obtain phase separation of the constituent components, respectively. Following evaporation, component parts were weighed. Confocal microscopy was performed at predetermined timepoints to examine the architecture of the nested nanoparticles. Briefly, nested nanoparticles were mounted onto a microscope slide for fluorescence examination using an upright inverted Nikon A1 confocal microscope (Nikon Instruments, Melville, NY), equipped with a 20× and 60× oil-immersion objective. Nikon Elements v4.1 software (Nikon Instruments, Melville, NY) was used for image processing.

Release Kinetics from Nested Nanoparticles: Fluorophore release was determined according to a previously published procedure.[27] Absorbance of bodipy and rhodamine were detected using a Synergy H4 Hybrid Reader as described above. In a separate study, nanoparticles were centrifuged at predetermined timepoints, resuspended in water, and the surface charge determined via zeta potential analysis, as described above.

Cytotoxicity Examination of Nested Nanoparticles: Cytotoxicity was determined via MTT assay using a CellTiter 96 Assay (Promega Corp., Madison, WI). Briefly, 10 000 human primary endothelial cells were seeded onto a 96-well plate. After 24 h, cells were treated with increasing doses of PLGA nanoparticles and nested nanoparticles. Plates were then incubated at 37 °C for 24 h in a CO_2 incubator. After incubation, cells were carefully washed 3 times with PBS. Dye Solution was added to all the wells and incubated for 4 h. After incubation, Solubilization Solution/Stop Mix was added to all wells followed by overnight incubation at 4 °C. Readings were taken using an Infinite 200 Pro plate reader (Tecan, Männedorf, CH) at wavelengths of 570 nm (reference wavelength 650 nm).

Nested Nanoparticle Internalization and Intracellular Release Following Incubation with MCF-7 Breast Cancer Cells: MCF-7 cells were seeded and kept in culture until 50% confluency. Cells were then incubated with nanoparticles, and at predetermined timepoints, samples were fixed with 4% methanol-free paraformaldehyde and permeabilized with 0.1% Triton-X 100 in PBS. Cells were washed, and stained with a solution containing 0.5 unit μL^{-1} of Alexa Fluor 555-conjugated phalloidin (Molecular Probes, Life Technologies, Grand Island, NY) at RT. Nuclei were stained with Vectashield mounting media with DAPI (Vector Laboratories, Burlingame, CA). Slides were mounted and examined via confocal microscopy as described above. For experiments involving flow cytometry analysis, cells were seeded and 24 h later incubated with nanoparticles. At predetermined timepoints, cells were collected, fixed, and resuspended in PBS. Fluorescence within cells was determined by side scatter measurements using a BD LSRFortessa Flow Cytometer (BD Biosciences, San Jose, CA), equipped with a 561 and 630 nm laser. BD FACSDiva software (BD Biosciences, San Jose, CA) was used for acquisition and data analysis.

In Vivo Accumulation and Release of Nested Nanoparticles in Breast Tumors: All animal experiments were approved by the UT MD Anderson Cancer Center Institutional Animal Care and Use Committee. MCF-7 cells (5×10^6) were inoculated in the mammary fat pads of 4- to 6-week–old female nude mice. Mice were implanted with 17β-estradiol pellets subcutaneously. Nanoparticles were administered intravenously and at predetermined timepoints, the mouse was sacrificed and the tumor harvested. Tumor tissues were frozen and sectioned into 7 μm tissue slices using an HM 550 Cryostat (Thermo Fischer Scientific, Waltham, MA). Tissues were fixed with 4% methanol-free paraformaldehyde for 20 min. Following fixation, samples were washed with PBS. Slides were mounted and tissues imaged using confocal microscopy as previously described. The presence of fluorescence over time, surface intensity plots, and area fraction of the tissue sections were examined using Nikon Elements v4.1 software. For area fraction analysis, the fluorescence emitted by bodipy and rhodamine was obtained from 4 sections from different regions of the tumor ($n = 3$). A ratiometric percentage of area fractions of both fluorophores were extracted from the total area of the image.

Statistical Analysis: All results comprise means, while error bars represent standard deviations. Statistics were calculated using GraphPad Prism software. Comparison between two groups was determined using one-way ANOVA followed by F-test, where $p < 0.01$ was significant.

Supporting Information

Supporting Information is available from the Wiley Online Library or from the author.

Acknowledgements

G.U.R.-E. and S.W. contributed equally to this research. F.M.-B., M.F., and E.B. share senior authorship. The authors appreciate the assistance of James Barrish (Texas Children's Hospital) in conducting TEM, Jianhua Gu (HMRI) for assistance with AFM, and David L. Haviland (HMRI) for flow cytometry analysis. Matthew G. Landry is acknowledged for manuscript schematics. This work was supported by a CDMRP Department of Defense Breast Cancer Research Program (DOD/BCRP) grant (W81XWH-11-1-0103) to E.B., who is also grateful for a Susan G. Komen Breast Cancer Foundation grant (KG101394). G.U.R.-E. and V.S.-I. acknowledge support from the Instituto Tecnológico y de Estudios Superiores de Monterrey. V.S.-I. also appreciates the support from the Consejo Nacional de Ciencia y Tecnología (CONACyT, 490202/278979).

Received: January 2, 2014
Revised: February 13, 2014
Published online:

[1] a) D. J. Butters, D. Ghersi, N. Wilcken, S. J. Kirk, P. T. Mallon, *Cochrane Database Syst. Rev.* **2010**, CD003368; b) D. Miles, G. von Minckwitz, A. D. Seidman, *The Oncologist* **2002**, *7*, 13.
[2] a) M. J. Lee, A. S. Ye, A. K. Gardino, A. M. Heijink, P. K. Sorger, G. MacBeath, M. B. Yaffe, *Cell* **2012**, *149*, 780; b) W. H. Mondesire, W. Jian, H. Zhang, J. Ensor, M. C. Hung, G. B. Mills, F. Meric-Bernstam, *Clin. Cancer Res.* **2004**, *10*, 7031.
[3] N. McCarthy, *Nat. Rev. Cancer* **2012**, *12*, 449.
[4] K. A. Janes, H. C. Reinhardt, M. B. Yaffe, *Cell* **2008**, *135*, 343.
[5] K. Galoian, H. T. Temple, A. Galoyan, *Tumour Biol.* **2012**, *33*, 885.
[6] a) A. Hamilton, L. Biganzoli, R. Coleman, L. Mauriac, P. Hennebert, A. Awada, M. Nooij, L. Beex, M. Piccart, I. Van Hoorebeeck, P. Bruning, D. de Valeriola, *Ann. Oncol.* **2002**, *13*, 910; b) A. Sparreboom, C. D. Scripture, V. Trieu, P. J. Williams, T. De, A. Yang, B. Beals, W. D. Figg, M. Hawkins, N. Desai, *Clin. Cancer Res.* **2005**, *11*, 4136.
[7] L. D. Mayer, T. O. Harasym, P. G. Tardi, N. L. Harasym, C. R. Shew, S. A. Johnstone, E. C. Ramsay, M. B. Bally, A. S. Janoff, *Mol. Cancer Ther.* **2006**, *5*, 1854.

[8] A. Gabizon, H. Shmeeda, Y. Barenholz, *Clin. Pharmacokin.* **2003**, *42*, 419.
[9] W. J. Gradishar, *Expert Opin. Pharmacother.* **2006**, *7*, 1041.
[10] M. E. Davis, Z. G. Chen, D. M. Shin, *Nat. Rev. Drug Discovery* **2008**, *7*, 771.
[11] a) M. Ferrari, *Nat. Rev. Cancer* **2005**, *5*, 161; b) D. Peer, J. M. Karp, S. Hong, O. C. Farokhzad, R. Margalit, R. Langer, *Nat. Nanotechnol.* **2007**, *2*, 751.
[12] a) H. Wang, Y. Zhao, Y. Wu, Y. L. Hu, K. Nan, G. Nie, H. Chen, *Biomaterials* **2011**, *32*, 8281; b) X. Dong, C. A. Mattingly, M. T. Tseng, M. J. Cho, Y. Liu, V. R. Adams, R. J. Mumper, *Cancer Res.* **2009**, *69*, 3918.
[13] a) E. J. Feldman, J. E. Lancet, J. E. Kolitz, E. K. Ritchie, G. J. Roboz, A. F. List, S. L. Allen, E. Asatiani, L. D. Mayer, C. Swenson, A. C. Louie, *J. Clin. Oncol.* **2011**, *29*, 979; b) J. R. Hasenstein, H. C. Shin, K. Kasmerchak, D. Buehler, G. S. Kwon, K. R. Kozak, *Mol. Cancer Ther.* **2012**, *11*, 2233.
[14] a) Z. J. Deng, S. W. Morton, E. Ben-Akiva, E. C. Dreaden, K. E. Shopsowitz, P. T. Hammond, *ACS Nano* **2013**; b) S. Sengupta, D. Eavarone, I. Capila, G. Zhao, N. Watson, T. Kiziltepe, R. Sasisekharan, *Nature* **2005**, *436*, 568; c) E. Tasciotti, X. Liu, R. Bhavane, K. Plant, A. D. Leonard, B. K. Price, M. M. Cheng, P. Decuzzi, J. M. Tour, F. Robertson, M. Ferrari, *Nat. Nanotechnol.* **2008**, *3*, 151.
[15] a) F. Danhier, E. Ansorena, J. M. Silva, R. Coco, A. Le Breton, V. Preat, *J. Controlled Release* **2012**, *161*, 505; b) J. K. Vasir, V. Labhasetwar, *Adv. Drug Delivery Rev.* **2007**, *59*, 718.
[16] a) M. E. Davis, M. E. Brewster, *Nat. Rev. Drug Discovery* **2004**, *3*, 1023; b) T. Loftsson, M. E. Brewster, *J. Pharm. Sci.* **2012**, *101*, 3019; c) V. J. Stella, Q. He, *Toxicol. Pathol.* **2008**, *36*, 30.
[17] C. M. Yam, Z. Xiao, J. Gu, S. Boutet, C. Cai, *J. Am. Chem. Soc.* **2003**, *125*, 7498.
[18] R. Zhu, S. Howorka, J. Proll, F. Kienberger, J. Preiner, J. Hesse, A. Ebner, V. P. Pastushenko, H. J. Gruber, P. Hinterdorfer, *Nat. Nanotechnol.* **2010**, *5*, 788.
[19] S. M. Moghimi, A. C. Hunter, J. C. Murray, *Pharmacol. Rev.* **2001**, *53*, 283.
[20] H. Cabral, Y. Matsumoto, K. Mizuno, Q. Chen, M. Murakami, M. Kimura, Y. Terada, M. R. Kano, K. Miyazono, M. Uesaka, N. Nishiyama, K. Kataoka, *Nat. Nanotechnol.* **2011**, *6*, 815.
[21] Q. H. Sun, M. Radosz, Y. Q. Shen, *J. Controlled Release* **2012**, *164*, 156.
[22] P.-O. Gendron, F. Avaltroni, K. Wilkinson, *J. Fluorescence* **2008**, *18*, 1093.
[23] a) J. Araujo, E. Vega, C. Lopes, M. A. Egea, M. L. Garcia, E. B. Souto, *Colloids Surf. B Biointerfaces* **2009**, *72*, 48; b) S. Yandrapu, U. B. Kompella, *J. Ocul. Pharmacol. Ther.* **2013**, *29*, 236.
[24] a) D. S. Jain, R. B. Athawale, A. N. Bajaj, S. S. Shrikhande, P. N. Goel, Y. Nikam, R. P. Gude, *Daru* **2014**, *22*, 18; b) X. Zhang, Y. Dong, X. Zeng, X. Liang, X. Li, W. Tao, H. Chen, Y. Jiang, L. Mei, S. S. Feng, *Biomaterials* **2014**, *35*, 1932.
[25] a) S. Ferrati, A. Mack, C. Chiappini, X. Liu, A. J. Bean, M. Ferrari, R. E. Serda, *Nanoscale* **2010**, *2*, 1512; b) R. Qi, S. Liu, J. Chen, H. Xiao, L. Yan, Y. Huang, X. Jing, *J. Controlled Release* **2012**, *159*, 251.
[26] C. Stigliano, S. Aryal, M. D. de Tullio, G. P. Nicchia, G. Pascazio, M. Svelto, P. Decuzzi, *Mol. Pharmaceutics* **2013**, *10*, 3186.
[27] K. A. Woodrow, Y. Cu, C. J. Booth, J. K. Saucier-Sawyer, M. J. Wood, W. M. Saltzman, *Nat. Mater.* **2009**, *8*, 526.